Domain boundary formation in helical multishell gold nanowires

2009 J. Phys.: Condens. Matter 21 272201

(http://iopscience.iop.org/0953-8984/21/27/272201)

IOP FTC
IOP Publishing
Journal of Physics: Condensed Matter
J. Phys.: Condens. Matter **21** (2009) 272201 (7pp)
doi:10.1088/0953-8984/21/27/272201

FAST TRACK COMMUNICATION

Domain boundary formation in helical multishell gold nanowires

T Hoshi[1,2] **and T Fujiwara**[2,3]

[1] Department of Applied Mathematics and Physics, Tottori University, Tottori 680-8550, Japan
[2] Core Research for Evolutional Science and Technology, Japan Science and Technology Agency (CREST-JST), Japan
[3] Center for Research and Development of Higher Education, The University of Tokyo, Bunkyo-ku, Tokyo, 113-8656, Japan

E-mail: hoshi@damp.tottori-u.ac.jp

Received 11 March 2009, in final form 22 May 2009
Published 4 June 2009
Online at stacks.iop.org/JPhysCM/21/272201

Abstract
Helical multishell gold nanowires are studied theoretically for the formation mechanism of the helical domain boundary. Nanowires with a wire length of more than 10 nm are relaxed by quantum mechanical molecular dynamics simulation with a tight-binding form Hamiltonian. In the results, non-helical nanowires are transformed into helical ones with the formation of atom pair defects at the domain boundary, where the defective atom pair is moved from an inner shell. Analysis of local electronic structure shows a competitive feature of the energy gain of reconstruction on the wire surface and the energy loss of the defect formation. A simple energy scaling theory gives a general explanation of domain boundary formation.

M This article features online multimedia enhancements

(Some figures in this article are in colour only in the electronic version)

1. Introduction

Nanometer scale material forms exotic structures and it is crucial to understand and control their formation mechanism, so as to establish the foundation of nano-electronics. Helical multishell gold nanowire [1, 2] is one of the exotic metal nanostructures [3] and has characteristic multishell configurations with 'magic numbers'. The helical wires were synthesized by focusing an electron beam on a thin film [4]. The wire axis is in the [110] direction of the original FCC structure and the outermost shell is a folded (111)-type (hexagonal) atomic sheet with helicity. A single shell helical structure was synthesized later [5]. The transport property was studied theoretically [6] and experimentally [7]. Platinum nanowires were also synthesized with the same type of helicity [8].

The observed multishell structures of the helical gold nanowires [1] are denoted by the numbers of atoms in each shell and are classified into 7–1, 11–4, 13–6, 14–7–1, and 15–8–1 structures. For example, a '14–7–1 nanowire' is a nanowire with three shells, and the outer, middle and inner shells have 14, 7 and 1 atom(s) in the section view, respectively. These numbers are called 'magic numbers', since the difference of the numbers between the outermost and next outermost shells is seven, except for the case of the 7–1 structure.

Theoretical investigations were carried out for the helical nanowire structures [9–12, 14, 13, 15–17] and, among them, a recent theory [15, 18] explains the observed multishell configuration with 'magic numbers' systematically. The theory was proposed as a two-stage formation model of helical multishell gold nanowires and the model was confirmed by quantum mechanical molecular dynamics simulations with tight-binding form Hamiltonians. The simulation shows the energy relaxation process from non-helical structures into helical ones. For comparison, a copper nanowire was simulated with the same conditions as gold and helical structure did not appear. The analysis of electronic structure concluded that the

origin of the helicity comes from the intrinsic nature of non-spherical 5d electrons and a (111)-type (hexagonal) surface structure is energetically favorable for 5d electrons in sheet structure. The above mechanism gives a general understanding of (i) the appearance of helical nanowire structures of gold and platinum and (ii) the fact that reconstructed equilibrium surfaces of FCC 5d metals, gold, platinum and iridium, prefer (111)-type structures [19–25]. After the theory paper [15], several related simulations were carried out for formation of a helical gold nanowire within a tight-binding form Hamiltonian [16, 17].

The present paper investigates the formation of a helical domain boundary on the wire surface, where the fundamental picture and simulation method are shared with the previous theory paper [15]. In general, a defect should be introduced at the domain boundary in the formation process of a helical domain from a non-helical one. The domain boundary was not discussed in the previous paper, since the simulated structures are short isolated wires of which the wire length is less than 3 nm. In the resultant helical nanowires, the domain boundaries are located in the wire ends, that are terminated artificially. In the present paper, simulations are carried out with longer wires, longer than 10 nm, and reveal a possible defect induced mechanism for forming the helical domain boundary.

This paper is organized as follows; section 2 describes the methodology and result of the simulation. Section 3 focuses on the analysis of the results, particularly on the energy per atom and the local density of states (LDOS). In section 4, a simple energy scaling theory with respect to the wire length of the helical domain is constructed for a general mechanism of domain boundary formation. Finally, the summary and future aspects are given in section 5.

2. Simulation

The formation process of the helical wires is realized by quantum mechanical molecular dynamics simulation as a structure relaxation with thermal fluctuation. The temperature was set to be $T = 600$ K, lower than the melting temperature (1337 K). The simulation code used here has the name of 'ELSES' (=extra-large-scale electronic structure calculations) [26–33, 15, 16, 34, 35]. The simulation was realized with a tight-binding form Hamiltonian [36–38], which was used for gold nanowire [40, 41, 39, 15–17]. The Hamiltonian form contains several parameters and they are determined to represent electronic structures of bulk solids, surfaces, stacking faults and point defects. One iteration step corresponds to $\Delta t = 1$ fs. The eigenstate calculation for the electronic structure is carried out at each iteration step. The boundary condition is imposed by fixing the mass center of the wire end layers [15]. The computational time with 608 atoms is typically nine minutes per iteration step, when a workstation with four dual-core Opteron™ processors was used.

We should say that the present simulation is different from experiment in several points. For example, the simulated time is quite short, 7–9 ps, owing to the practical limit of the computational resources. Therefore, the simulation result should be understood so that it captures an intrinsic energetic mechanism of the real process.

The transformation process is depicted in figure 1(a) for the 11–4 structure, which will be analyzed throughout this paper. The process for the 15–8–1 structure [16] is also depicted in figure 1(b). The initial structures are parts of ideal FCC structure and are the same as those in the previous paper, except their wire length. The wire length of these nanowires is approximately 12 nm. The wire has 40 or 42 unit layers in the wire axis direction for the 11–4 and 15–8–1 structures, respectively. Here a unit layer of a [110] nanowire consists of two successive atom layers.

The basic transformation mechanism is common among the present results (longer wires) and the previous ones (shorter wires) [15] and is shown schematically in figures 1(c) and (d) in the case of the 7–1 structure. A section view of the initial structure is depicted in figure 1(c) with the labels, α, β and γ, for several atoms. Expanded lateral surfaces are depicted in figure 1(d) for the initial (left) and final (right) structures. In the initial structures, the wire surface consists of (111)-type (hexagonal) and (001)-type (square) areas. The latter area consists of two atom rows and the atoms in the area are drawn as filled squares, such as α and β, in figures 1(c) and (d). The two atom rows are indicated by the two parallel arrows in figures 1(a) and (b). Figure 1(d) shows a shear-like transformation in which the square-lattice area is transformed into the hexagonal-lattice one. In the result, the wire axis is slightly tilted from the original [110] direction, as seen in the right panel of figure 1(d), and the helicity is introduced. The geometrical relation between the tilt angle and the helicity is discussed in figure 3(A) of [1].

The nanowires of figures 1(a) and (b), unlike the shorter ones [15], contain multiple helical domains with well defined domain boundary, which will be focused on hereafter.

Figure 2 shows several snapshots of side view for the 11–4 case, where the atoms are distinguished by color, so as to clarify the transformation process. Red atoms are those initially placed on the (001)-type surface area and green atoms are those initially placed in the inner shell region. The other atoms are those initially placed on the (111)-type surface area. The central region indicated by broken lines in figures 2(a)–(d) is sketched in figures 2(e)–(g). Figures 2(e) and (f) capture the structures of figures 2(a) and (b), respectively, and figure 2(g) captures the structure of figure 2(c) or (d). In the initial structure, figure 2(e), the 'red' atoms, marked as P, Q, V, W, X and Y, form a square lattice on the wire surface, and the 'green' atoms, marked as R and S, are placed in the inner shell. In the final snapshot, figure 2(g), the two 'green' atoms, R and S, are moved from the inner shell into the wire surface, and form a helical domain boundary. They are inserted between atoms P and V, while atom Q is moved into an upper area between atoms T and U. As a result, the surface reconstruction occurs, from the (001)-type (square) lattice into the (111)-type (hexagonal) one, and introduces the helical domains with domain boundaries.

As a remarkable tendency of the entire sample, pairs of 'green' atoms are moved from the inner shell into the region of 'red' atom rows on the surface, as illustrated in figures 2(h)

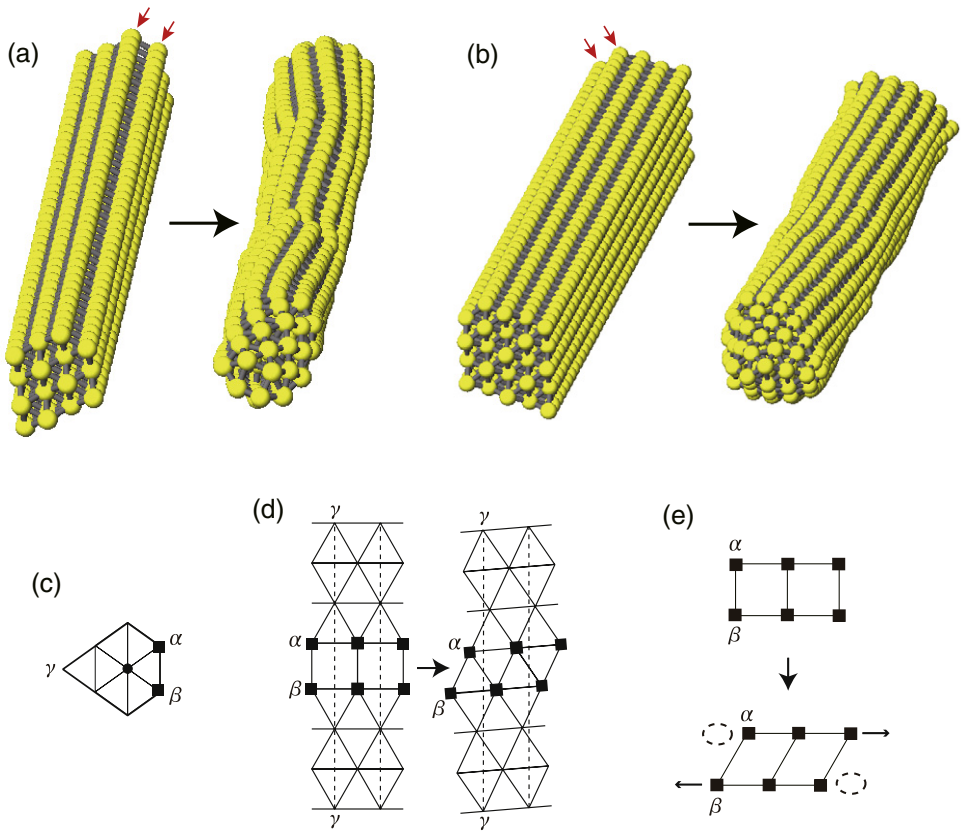

Figure 1. (a), (b) Simulated formation process of helical multishell gold nanowires with wire lengths longer than 10 nm. The 11–4 structure (a) is depicted in the initial structure (left panel) and the 9000th iteration step (right panel). The 15–8–1 structure (b) [16] is depicted in the initial structure (left panel) and the 6600th iteration step (right panel). (c), (d) Schematic figures of the formation process for the 7–1 structure. The section view of the initial structure is depicted in (c), where several atoms are labeled α, β and γ. (d) Expanded lateral surface of the 7–1 structure in the initial (left) and final (right) structures. Dashed lines connect the same atoms such as γ. (e) A simplified figure of the transformation process of (d). Only the atoms of the filled squares in (d) are drawn. Ovals of broken lines indicate possible vacant regions that are formed by the transformation. The supplementary movie files of movie-a.gif (available from stacks.iop.org/JPhysCM/21/272201) (1.1 MB) and movie-b.gif (available from stacks.iop.org/JPhysCM/21/272201) (1.5 MB) are available for (a) and (b), respectively.

and (i). The essential mechanism is depicted in figure 1(e), in which only the atoms of the filled squares in figure 1(d), or the 'red' atoms in figure 2, are drawn without the tilting freedom and the direction of the shear-like deformation is depicted as the arrows in the lower panel. When the shear-like deformation occurs within a finite domain drawn in figure 1(e), vacant regions are introduced, as depicted by ovals of broken lines in figure 1(e). The vacant regions are filled by atoms moved from the inner shell, so as to form a part of a hexagonal-lattice area on the surface. Therefore, the finite domain with the shear-like deformation forms a helical domain with the filled atoms at the domain boundary. Moreover, figure 2(i) shows that the shear-like deformation occurs in the opposite shear directions between neighboring domains and the atoms move typically as atom pairs, such as the pair of atoms R and S. Figure 2(g) indicates that the inserted atoms of R and S form part of a hexagonal-lattice area.

3. Analysis of local electronic structure

The transformation process from the non-helical wire into the helical one occurs with energy gain, according to the change of the total energy shown in figure 3(a).

The change of the atom energy, the energy of each atom, is plotted in figure 3(b) for the selected atoms P, Q, R and S that are indicated in figures 2(e)–(g). Figure 4(a) shows the LDOS of atom P in the initial structure and the 1000th and 9000th steps. Figure 4(b) shows the LDOS of atom R in the initial structure and the 1000th, 1300th and 9000th steps. In figure 4, the origin of the vertical axis is shifted among the snapshots and the origin of the horizontal axis is set to the Fermi level for each snapshot. Since the values of the Fermi level are different only about or within 0.1 eV among the snapshots, the difference in the Fermi level is negligible in the energy scale of the graphs. Since atom R is placed in the inner shell in the initial structure, the LDOS profile, shown in the lowest graph of figure 4(b), is similar to that of bulk FCC gold and has three characteristic peaks in the 5d band at $\varepsilon \approx -2$, -4 and -6 eV.

The atom movement from the inner shell into the wire surface accompanies the drastic change of the atom energy. Figure 3(b) contains temporal peaks nearly at the 1000th and 2400th iterations for atoms R and S, respectively, which corresponds to the successive atom movements of atoms R and S from the inner shell into the wire surface, shown in figure 2.

When the initial and final structures are compared in the atom energy, one can find that the helical transformation is

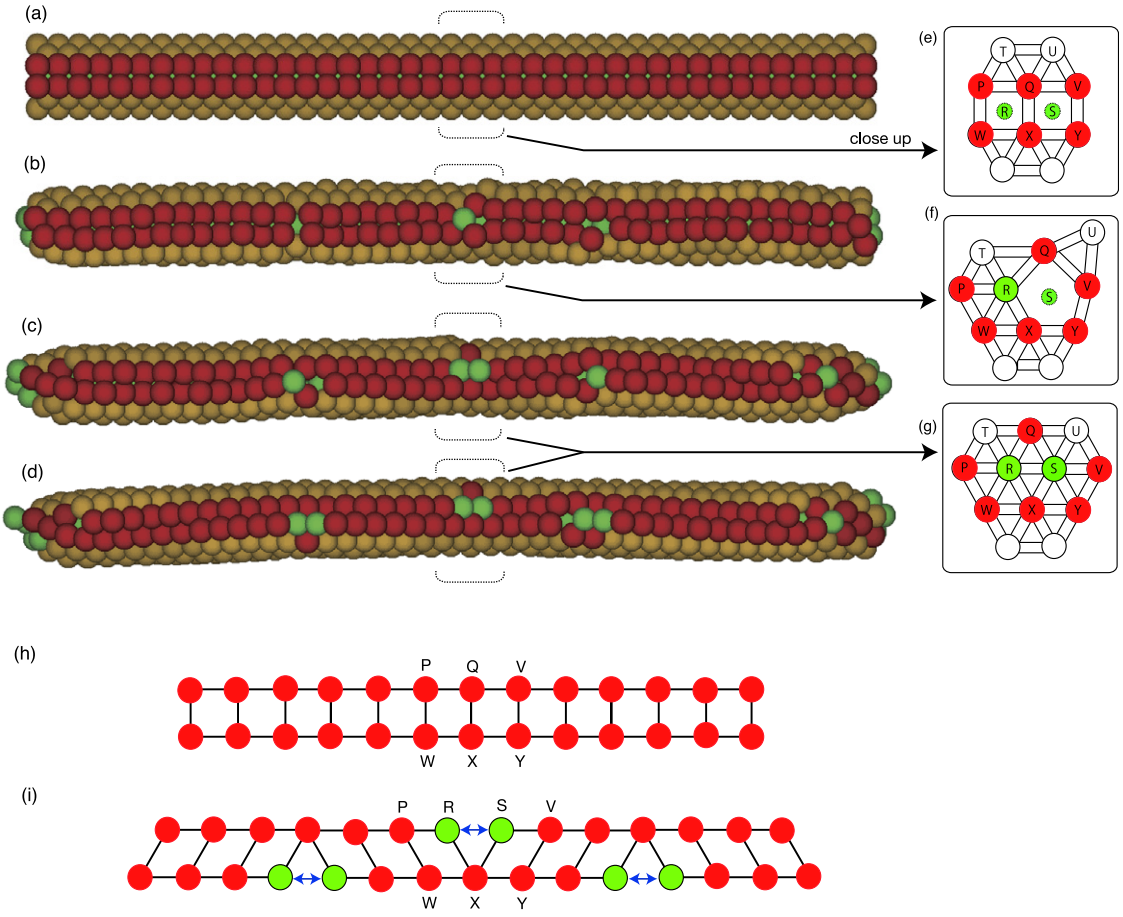

Figure 2. The transformation process of the 11–4 structure. (a)–(d) Snapshots in the initial structure and 1000th, 3000th and 9000th iteration steps, respectively. (e)–(g) Sketched figure as a close-up of the central area that is indicated by broken lines on the wire surface. (e) and (f) capture the structures of (a) and (b), respectively and (g) captures the structure of (c) or (d). The atoms depicted as smaller balls, R and S in (e) and S in (f), are placed within the inner shell. (h), (i) Schematic figure of formation of atom pair defects in the (h) initial and (i) final structures. The supplementary movie file of movie-c.gif (available from stacks.iop.org/JPhysCM/21/272201) (1.5 MB) is available for (a)–(d).

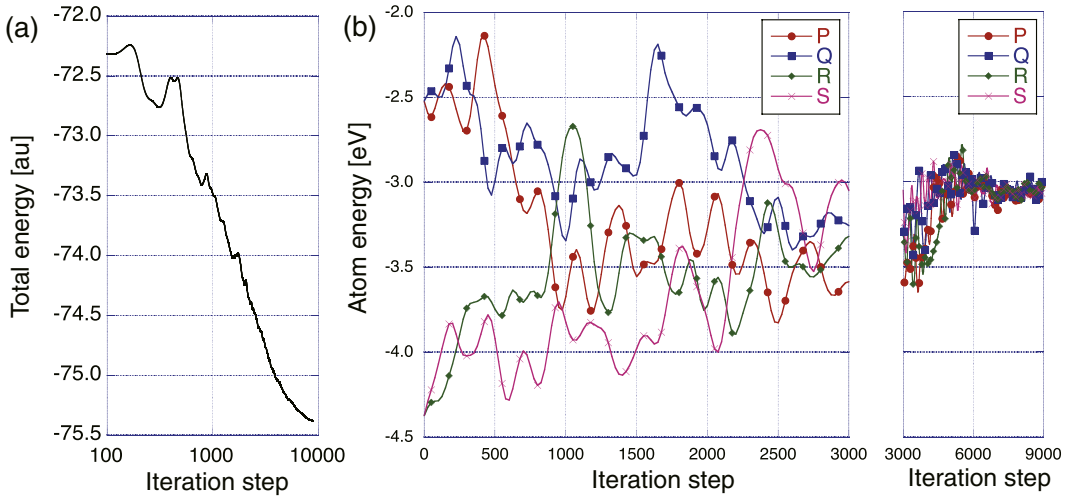

Figure 3. Energy change of the 11–4 structure during the relaxation process. (a) Change of the total energy. (b) Change of the atom energy for atoms P, Q, R and S that are indicated in figure 2.

induced by a surface effect. In the final iteration step (9000th iteration step), the four atoms P, Q, R and S are transformed into members of the folded (111)-type surface with helicity, as shown in figures 2(d) and (g). Therefore, their atom energy reaches an almost unique value, $E \approx -3.1$ eV in figure 3(b), and the final LDOS profiles of atoms P and R are

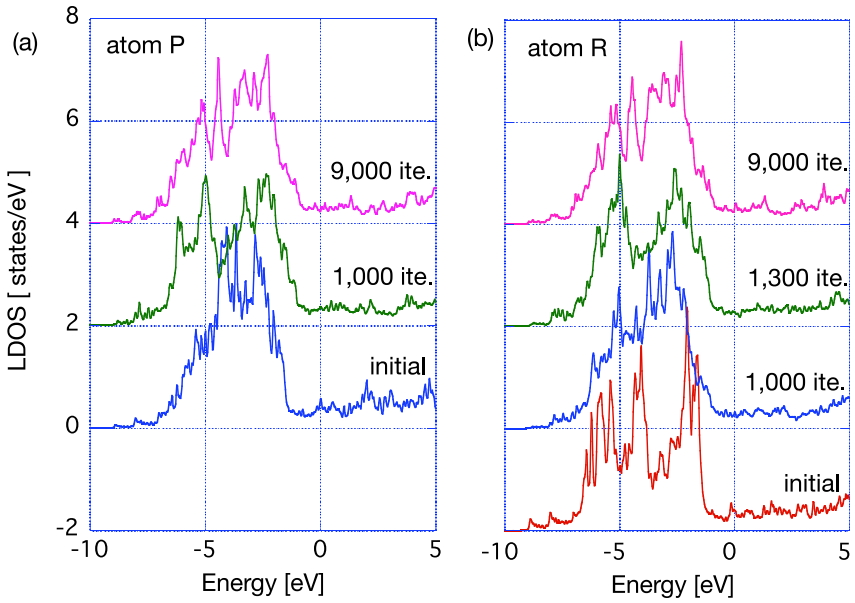

Figure 4. Local density of states of atoms P and R in the initial structure and several iteration steps written in the graphs. The origin of the vertical axis is shifted among different iteration steps. The origin of the horizontal axis is set to the Fermi level.

quite similar, as plotted in the highest graphs of figures 4(a) and (b). In figure 2, atoms P and Q, depicted as 'red' atoms, are transformed from the (001)-type surface area into the (111)-type one. Figure 3(b) shows that the atom energy of the two atoms decreases from $E \approx -2.5$ to -3.1 eV and the amplitude of the energy gain is $E_{\rm gain} \approx 0.6$ eV. The energy gain mechanism is explained by the two-stage model in the previous paper, and the present case corresponds to the case of atom B in the paper [15]. On the other hand, atoms R and S, depicted as 'green' atoms in figure 2, are moved from the inner shell into the (111)-type surface area. Figure 3(b) shows that the atom energy of the two atoms increases from $E \approx -4.3$ to -3.1 eV and the amplitude of the energy loss is $E_{\rm loss} \approx 1.2$ eV.

The above observation of the increase and decrease of the atom energy is confirmed when histograms (not shown) are constructed for the atom energy difference ΔE between the initial and final structures. The histograms are constructed among all the atoms except the 158 atoms located within the five layers near the two wire ends, so as to avoid possible artifacts of the wire ends. All the 'red' atoms, the atoms originally placed on the (001)-type area of the surface, show the energy decrease of $\Delta E \approx -0.2$ to -1.2 eV and the histogram peak is located at $\Delta E \approx -0.7$ eV. The 'green' atoms, the atoms originally placed in the inner shell, show the energy difference from $\Delta E \approx -0.2$ to 1.6 eV. The large energy increase ($\Delta E \approx 1.2$ to 1.6 eV) comes from the atoms moved into the wire surface, like atoms R and S. An energy increase also appears among several other 'green' atoms in the inner shell, since the resultant helical wire has defective regions in the inner shell, particularly regions near the moved atoms. The histogram of the remaining atoms, the atoms originally placed on the (111)-type area of the surface, shows a wide range of values $\Delta E \approx -1.2$ to 1.0 eV and their average is an energy decrease ($\Delta E \approx -0.16$ eV). We should remember that these 'remaining' atoms are different in their situations in the initial structure. See the cases of atoms A and C in the previous paper [15].

It should be noted that an experimental paper on a [110] gold nanowire [4], earlier than the report of helical structure [1], suggests a surface stabilization mechanism in which (001)-type areas on the wire surface reconstruct into (111)-type ones as on the equilibrium surface. The suggested stabilization mechanism is consistent with the previous theory [15] and the present analysis.

The analysis of the intermediate structures reveals a competitive feature of temporal energy gain and loss among atoms. In figure 3(b), for example, atom R shows an energy loss during the 800th and 1000th iteration steps ($E \approx -3.7$ eV $\Rightarrow -2.7$ eV), while atoms P and Q show an energy gain during the same period ($E \approx -3.1$ eV $\Rightarrow -3.7$ eV and $E \approx -2.8$ eV $\Rightarrow -3.4$ eV for P and Q respectively). The temporal energy gain and loss are of almost the same amplitude. During this period, atom R is moved from the inner shell to the wire surface (see figure 2(b)). In conclusion, atom R is moved with energy loss, from the inner shell into the wire surface, because of the energy gain mechanism of atoms P and R. The energy gain is also found in the LDOS profile of atom P, shown in figure 4(a). When the LDOS profile is compared between those in the initial structure and at the 1000th step, the weighted center of the 5d band is shifted downwards. Moreover a gap-like structure appears, at $\varepsilon \approx -4.5$ eV, in the LDOS profile of the 1000th step, which indicates the formation of bonding and antibonding states. In short, an unstable surface atom is changed into a (relatively) stable one, owing to the energy gain of the 5d electrons [15]. Atom R also shows a temporal energy gain after the movement into the wire surface, during the period between the 1000th and 1300th iterations ($E \approx -2.7$ eV $\Rightarrow -3.8$ eV). The change of the LDOS profile during this period, shown in figure 4(b), is similar to the change of

atom P discussed above, which indicates the same stabilization mechanism with the 5d electrons.

4. Discussion

Here a simple energy scaling theory is constructed with respect to the number of unit layers for a helical domain $n_{\rm dom}$ and gives the lower limit of realistic domain length. The analysis of section 3 is summarized as the competition between the energy gain within the helical domain and the energy loss at the domain boundary. The former quantity is proportional to the number of layers for a domain ($O(n_{\rm dom})$) and the latter is independent of the number of layers ($O(1)$). The realistic domain length should be so long that the energy gain is dominant.

The main energy gain comes from the surface reconstruction of the 'red' atoms in figure 2. The energy gain per atom is estimated to be $E_{\rm gain} \approx 0.6$ eV by the analysis in section 3. The main energy loss, on the other hand, comes from the 'green' atoms that appear at domain boundary on the wire surface. The energy loss per atom is estimated to be $E_{\rm loss} \approx 1.2$ eV by the analysis in section 2. The energy gain per unit layer is estimated to be $2E_{\rm gain}$, since one unit layer of the wire contains two 'red' atoms. The energy loss at the domain boundary is estimated to be $2E_{\rm loss}$, since the defect appears typically as an atom pair. The energy difference between the initial and final structures is modeled as

$$\Delta E_{\rm wire} = -2E_{\rm gain}n_{\rm dom} + 2E_{\rm loss}, \qquad (1)$$

and a helical domain should appear in the case of $\Delta E_{\rm wire} < 0$. The realistic domain length should be long enough to satisfy $n_{\rm dom} > n_{\rm dom}^{\rm (c)} \equiv (2E_{\rm loss})/(2E_{\rm gain}) = 2$.

The above estimation is consistent with the domain structure of figure 2(d), since the number of layers for a resultant helical domain is larger than two. If the number of layers for a simulated wire is less than ten, multiple domains with the domain boundary are not formed [15]. It is noteworthy that, for a short wire in the 12–6–1 structure [15], the atom movement from the inner shell into the wire surface was found and the movement occurs within one atom row, not within one atom pair.

The present simulation gives two conclusive points for the formation of a helical gold nanowire. (i) The mechanism of atom insertion on the surface, which introduces the helical domain and domain boundary with point defects. (ii) The simple energy scaling theory that explains the net energy gain. The above two points are universal and not dependent on the details of simulations. In general, the inserted atom can be supplied not only from the inner shell but also from the outer area [15]. We speculate that another candidate for the source of the atom supply is the wire ends, if they are connected to electrode parts.

5. Summary and future work

In summary, domain boundary formation is explored for a helical multishell gold nanowire. The simulations were carried out for nanowires longer than 10 nm by quantum mechanical molecular dynamics simulation. As results, the shear-like deformation on the (001)-type surface area introduces helical domains [15] and a domain boundary appears, typically with the supply of a defective atom pair from the inner shell, between two domains with the opposite shear directions. The mechanism is explained quantitatively by the analysis of local electronic structure and a general discussion is given using a simple energy scaling theory.

As future work, simulations should be carried out with larger samples that contain electrode parts, as pointed out above. We note that the simulation with realistic electrodes is also important for the transport property, particularly among helical multishell nanowires and other nanowires thicker than a monatomic chain, because of the possible interference effect at the connection with the electrodes [42, 6, 7, 43, 44].

A promising theoretical approach for larger quantum mechanical simulations is the 'order-N' method, in which the computational time is 'order N', or proportional to the system size N. See articles cited in [33] or a recent journal volume that includes [16] and focuses on the order-N methods.

References

[1] Kondo Y and Takayanagi K 2000 *Science* **289** 606
[2] Oshima Y, Kondo Y and Takayanagi K 2003 *J. Electron Microsc.* **52** 49
[3] Agraït N, Yeyati A L and van Ruitenbeek J M 2003 *Phys. Rep.* **377** 81
[4] Kondo Y and Takayanagi K 1997 *Phys. Rev. Lett.* **79** 3455
[5] Oshima Y, Onga A and Takayanagi K 2003 *Phys. Rev. Lett.* **91** 205503
[6] Ono T and Hirose K 2005 *Phys. Rev. Lett.* **94** 206806
[7] Oshima Y, Mouri K, Hirayama H and Takayanagi K 2006 *J. Phys. Soc. Japan* **75** 053705
[8] Oshima Y, Koizumi H, Mouri K, Hirayama H, Takayanagi K and Kondo Y 2002 *Phys. Rev.* B **65** 121401(R)
[9] Gülseren O, Ercolessi F and Tosatti E 1998 *Phys. Rev. Lett.* **80** 3775
[10] Tosatti E, Prestipino S, Kostlmeier S, Dal Corso A and Di Tolla F D 2001 *Science* **291** 288
[11] Bilalbegović G 2003 *Vacuum* **71** 165
[12] Senger R T, Dag S and Ciraci S 2004 *Phys. Rev. Lett.* **93** 196807
[13] Lin J-S, Ju S-P and Lee W-J 2005 *Phys. Rev.* B **72** 085448
[14] Yang C-K 2004 *Appl. Phys. Lett.* **85** 2923
[15] Iguchi Y, Hoshi T and Fujiwara T 2007 *Phys. Rev. Lett.* **99** 125507
[16] Fujiwara T, Hoshi T and Yamamoto S 2008 *J. Phys.: Condens. Matter* **20** 294202
[17] Amorim E P M and da Silva E Z 2008 *Phys. Rev. Lett.* **101** 125502
[18] Iguchi Y 2007 *D. Thesis* University of Tokyo, Tokyo (in Japanese)
[19] Fedak D G and Gjostein N A 1967 *Acta Metal.* **15** 827
[20] Binnig G, Rohrer H, Gerber Ch and Weibel E 1983 *Surf. Sci.* **131** L379
[21] Ho K-M and Bohnen K P 1987 *Phys. Rev. Lett.* **59** 1833
[22] Van Hove M A, Koestner R J, Stair P C, Biberian J P, Kesmodel L L, Bartos I and Somorjai G A 1981 *Surf. Sci.* **103** 189
[23] Binnig G, Rohrer Gerber C and Stall E 1984 *Surf. Sci.* **144** 321
[24] Abernathy D L, Mochrie S G J, Zehner D M, Grübel G and Gibbs D 1992 *Phys. Rev.* B **45** 9272

[25] Jahns V, Zehner D M, Watson G M and Gibbs D 1999 *Surf. Sci.* **430** 55
[26] http://www.elses.jp/
[27] Hoshi T and Fujiwara T 2000 *J. Phys. Soc. Japan* **69** 3773
[28] Hoshi T and Fujiwara T 2003 *J. Phys. Soc. Japan* **72** 2429
[29] Geshi M, Hoshi T and Fujiwara T 2003 *J. Phys. Soc. Japan* **72** 2880
[30] Takayama R, Hoshi T and Fujiwara T 2004 *J. Phys. Soc. Japan* **73** 1519
[31] Hoshi T, Iguchi Y and Fujiwara T 2005 *Phys. Rev.* B **72** 075323
[32] Takayama R, Hoshi T, Sogabe T, Zhang S-L and Fujiwara T 2006 *Phys. Rev.* B **73** 165108
[33] Hoshi T and Fujiwara T 2006 *J. Phys.: Condens. Matter* **18** 10787
[34] Yamamoto S, Hoshi T, Sogabe T, Zhang S-L and Fujiwara T 2008 *J. Phys. Soc. Japan* **77** 114713
[35] Hoshi T and Fujiwara T 2009 *J. Phys.: Condens. Matter* **21** 064233
[36] Mehl M J and Papaconstantopoulos D A 1996 *Phys. Rev.* B **54** 4519
[37] Kirchhoff F, Mehl M J, Papanicolaou N I, Papaconstantopoulos D A and Khan F S 2001 *Phys. Rev.* B **63** 195101
[38] Papaconstantopoulos D A and Mehl M J 2003 *J. Phys.: Condens. Matter* **15** R413
[39] Haftel M I and Gall K 2006 *Phys. Rev.* B **74** 035420
[40] da Silva E Z, da Silva A J R and Fazzio A 2001 *Phys. Rev. Lett.* **87** 256102
[41] da Silva E Z, Novaes F D, da Silva A J R and Fazzio A 2004 *Phys. Rev.* B **69** 115411
[42] Oshima Y, Mouri K, Hirayama H and Takayanagi K 2003 *Surf. Sci.* **531** 209
[43] Kurui Y, Oshima Y, Okamoto M and Takayanagi K 2008 *Phys. Rev.* B **77** 161403(R)
[44] Shinaoka H, Hoshi T and Fujiwara T 2008 *J. Phys. Soc. Japan* **77** 114712